Real-Time Implementation of The Fuzzy Logic Controlled Parallel Protection Technique to Enhance the DFIG System's Fault Ride Through Capability

*Aftab Ahmed Ansari, Giribabu Dyanamina

[1,2] Maulana Azad National Institute of Technology, Bhopal, India

Corresponding author: Aftab Ahmed Ansari[*]
Mobile No- +91 8878425322
E-mail: aftab786zakir@gmail.com
Postal Address- 62 Sector A Hazrat Nizamuddin Colony BHEL Bhopal, 462022
(M.P), INDIA

Abstract— Fault Ride through (FRT) capability is one of the critical needs mandated as per new grid regulations to accept large wind energy penetration into grid. In this paper, a hybrid approach has been proposed to improve the FRT of the grid-connected Doubly Fed Induction Generator fed wind energy conversion (DFIG-WEC) system using fuzzy approach. The proposed method has been designed by integrating the rotor side series dynamic braking resistor (RSDBR), the DC-link braking chopper (DCBC) and the rotor end parallel resistor crowbar (REPRC) topologies for limiting the peak values of the fault rotor current, stator current, and dc-link voltage, to protect the rotor-side converter, also reduce torque fluctuations, avoid frequent use of crowbar short-circuit, improve rotor-side converter operation time and the FRT capability. This research article also presents various fault overcurrent scenarios (symmetrical and asymmetrical) and provides protection analysis, including switching methods, coordination with different topologies, and resistance value calculations. The effectiveness of the proposed technique is verified using a MATLAB simulation mode for a DFIG system driven by a typical 1.5 MW wind turbine. The real-time simulator (RTS)-based OPAL-RT4500 effectively verifies the operation of the scheme under various fault conditions.
Keywords: *Doubly-fed induction generator (DFIG), Electrical Drives, Fault ride through, Fuzzy Logic, Power Electronics, Renewable energy system, Voltage dip, Wind energy conversion (WEC) system,*

1.   INTRODUCTION

The global energy crisis and Russia's use of energy as a geopolitical tool highlight the danger of relying on fossil fuels. The solution to climate change, energy security and affordability lies in a rapid shift to renewable energy. Wind energy is a crucial source that is leading the way, with the industry experiencing growth despite the COVID-19 pandemic. In 2020, 94 GW of capacity was built, making it the second-best year ever for the sector. The Global Wind Report predicts a growth of 1.8% lower in 2021, indicating the resilience and persistence of the wind energy industry [1].

Wind turbines can be classified as either fixed speed turbines (FST) or variable speed turbines (VST). FST is the earliest and simplest type of wind turbine, using a fixed-speed induction generator to produce electrical power. However, FST has limitations in operating efficiently in variable wind speeds. VST, on the other hand, uses a doubly-fed induction generator (DFIG) to produce electrical power. VST is more efficient than FST and can operate in a wider range of wind speeds. The rotor of the DFIG is connected to the grid through power electronics, allowing the rotor to be controlled independently from the grid, optimizing the system's performance under varying wind conditions. DFIG-based wind energy conversion (WEC) systems have several advantages over other WEC technologies. DFIG systems can provide reactive power support to the grid, helping maintain grid stability. These systems are highly reliable, have low maintenance requirements, and can operate in a wide range of wind speeds. A grid-connected DFIG system consists of a DFIG, power electronics, a transformer, and a grid connection. The DFIG converts mechanical energy from the wind into electrical energy, and the power electronics allow for the rotor to operate at variable speeds, optimizing performance. The stator of the DFIG is connected directly to the grid through a transformer, while the rotor is connected to the grid through a back-to-back converter (BTBC) [2]. The BTBC consists of two converters: a rotor-side power electronic converter (RSPEC) and a grid-side power electronic converter (GSPEC). The transformer steps up the voltage of the electrical energy produced by the DFIG to a level suitable for transmission over long distances [3]. However, vulnerability to grid disturbances is the most significant limitation of this configuration. Techniques have been proposed to enhance the DFIG fault ride-through (FRT) capacity during grid disturbances, either by enhancing control strategies or by adding external hardware circuits [4].

The hardware circuit solution includes protection circuits, storage devices, and reactive power injection devices, namely flexible AC transmission controllers (FACTS) [5]. Combinational circuit techniques with crowbar and chopper circuits are also studied in [6]. This protection circuit shields the RSPEC by shorting the rotor terminals, however, it converts the DFIG into a self-excited induction generator (SEIG), requiring reactive power from the grid. Fault current limiters (FCL) such as series dynamic braking resistors (SDBR) [7], superconducting fault current limiters (SFCL) [8] and switching fault current limiters (STFCL) [9] are other alternative hardware FRT enhancement mechanisms because they prevent disconnection of back-to-back converters. In addition, storage devices such as batteries [10], supercapacitors [11], flywheel energy storage [12], and combined

methods using Crowbar and SDBR with superconducting magnetic energy storage (SMES) [13] have been used to enhance the active power of the FRT capable network. Thermal runaway with high penetration and overcharging issues are some of the disadvantages of memory-based FRT technologies. They are prohibitively expensive and have low energy density. Further implementation of FACTS equipment in FRT operations requires highly rated switchgear and efficient controllers, which adds cost.

In addition to hardware-based techniques, improved software-based control methods have been proposed, such as blade pitch control [14], improved vector control of RSPEC [15], fuzzy logic control (FLC)[16], feed-forward transient current control [17], sliding mode control (SMC) [18] and model predictive control (MPC) [19] to improve transient stability during faults. The cost of improved software-based control methods is inexpensive, but the added complexity and limitations of fault currents make these FRT functions less attractive.

Effective utilization of existing hardware in a DFIG system will enhance the FRT capabilities. Therefore, a Fuzzy Logic (FL) controlled improved parallel protection scheme for DFIG based WEC system has been proposed in this paper by combining rotor end series dynamic braking resistor (RSDBR), the DC link braking chopper (DCBC), and the rotor end parallel resistance crowbar (REPRC) topologies. The three topologies that are part of the coordination topology are linked in different ways, but they are all controlled by a FL system. Implementing this coordinated approach with the coupled crowbars has advantages such as:

- The variation range of the dc-link Voltage is lowered after the improved control strategy has been used, which is an indication that the quick dynamic response has been attained. It takes longer for the dc voltage to stabilize in the scenario of REPRC operations alone.
- Despite the rotor crowbar being connected for a short time, the dc-link voltage remains stable. This demonstrates the significance of utilizing the proposed improved technique, as this combination can contribute in minimizing the dc voltage fluctuation during fault more quickly, hence decreases the rotor crowbar switching time.
- The generator will only run out of control for a short period of time because of that DFIG will not be used as a SEIG for a long time. This makes easier for generator to quickly manage their reactive power exchange with the grid.
- Proposed Coordinated technique reduces the magnitude of rotor and stator currents during fault conditions.
- The torque oscillation of the generator has less dampening, and the DFIG is able to export to the grid a greater amount of reactive power during the transition phase after the fault is cleared using proposed topology.

The effectiveness of the proposed protection technique was studied for several fault types, both symmetrical and asymmetrical, such as single-phase, two-phase, and three-phase ground faults. This paper's subsequent sections are structured as follows: Section 2 discusses the DFIG's behavior in symmetrical and asymmetrical faults. Section 3 introduces an Improved Parallel FL based converter protection mechanism that combines the RSDBR, DCBC, and the REPRC. As a result, Sections 4 simulate the Improved proposed parallel protective mechanism for the DFIG based WEC system in the MATLAB. Section 6 comprehends the RTS results; finally, the conclusions are outlined.

2. BEHAVIOR DURING VOLTAGE DIPS

This section presents the dynamic model of a DFIG during a grid failure, specifically examining how the model behaves when there are drops in voltage caused by both symmetrical and asymmetrical grid failures. The WEC system needs to maintain its connection to the power grid and provide reactive power compensation during grid outages. Grid faults often lead to a drop in voltage at the WEC system terminal. In a WEC system with a full-scale Power Electronic Converter (PEC), the generator is entirely isolated from the grid and won't directly experience the voltage loss. Therefore, the PEC's FRT capability determines the system's FRT capability. However, in a DFIG-fed WEC system, voltage sag affects both the grid-side power electronic converter (GSPEC) and the generator since the DFIG's stator is directly connected to the grid [20]. This makes the DFIG's job more challenging when the grid fails. Before investigating the DFIG's enhanced FRT method, it is essential to understand the DFIG's dynamic model during grid faults and evaluate the system's effectiveness during such events.

2.1 DFIG Equivalent Circuits During Voltage Sags

The mathematical formulation of a DFIG in alpha beta frame is rewritten in Equation (1-4), in order to examine the functionality of DFIG [20].

$$v_s = R_s i_s + \frac{d\psi_s}{dt} \tag{1}$$

$$v_r = R_r i_r + \frac{d\psi_r}{dt} - j\omega_r \psi_r \tag{2}$$

$$\psi_s = L_s i_s + M i_r \tag{3}$$

$$\psi_r = L_r i_r + M i_s \tag{4}$$

2

2.2 Symmetrical Voltage Sags

During a voltage sag, the stator flux of a DFIG can't change suddenly. To keep the flux continuous, a natural stator flux (ψ_{sn}) is added. Fig. 1 shows how the stator flux changes during a symmetrical-voltage drop of 80%. Before the voltage drop, the stator flux vector (ψ_s) moves with the grid voltage vector. When the voltage drops, the grid voltage vector's size reduces. But since the stator flux can't shift quickly (as per the principle of magnetic flux conservation), a natural flux (ψ_{sn}) emerges and moves with the grid voltage vector, as shown in Equation 5 and also in Fig. 1 [21] .

$$\psi_{sn}(t_0) = \frac{pV_s}{j\omega_s} \tag{5}$$

where p represents the level of voltage drop and ω_s represent grid frequency.

This results in a combination of two independent frequency components in the stator-flux. The stator's inherent flux (ψ_{sn}), makes up the first portion of the voltage drop, which is the delayed DC part of the stator's alpha-beta frame. Its rate of decay depends on how the DFIG works after the voltage drops. The stator-forced flux (ψ_{sf}) is another generated by the leftover grid voltage $v_s = (1-p)V_s e^{(j\omega_s t)}$, which rotates in synchronous with the grid frequency (ω_s)and grid voltage vector, as seen in Fig. 1(b).

The superposition principle can be used to describe the dynamic analysis of the DFIG under balanced voltage sags with two different equivalent circuits: the natural machine, in which the stator is short-circuited and the natural flux (ψ_{sn}) is present in the stator winding, and the forced-machine, in which the stator voltage is the remaining grid voltage and there is no transitory flux left, as shown in Fig. 2.

Under normal conditions, the equivalent-circuit of the forced machine is identical to the DFIG's standard operating circuit. Fig. 2(b) yields the distinct equation describing the relationship between stator natural-flux (ψ_{sn}) and rotor natural current (i_{rn}), as expressed in Equation (6) and (7):

$$\frac{d\psi_{sn}}{dt} = -\frac{R_S}{L_s}\psi_{sn} + \frac{L_S}{L_s}R_s i_{rn} \tag{6}$$

$$(\frac{d}{dt} - j\omega_r)\psi_{sn} = v_{rn} - R_r i_{rn} - (\frac{d}{dt} - j\omega_r)\sigma L_r i_{rn} \tag{7}$$

2.3 Asymmetrical Voltage Dips

The symmetrical component approach can be used to divide the asymmetrical grid voltage into positive, negative, and zero sequence components. The grid voltage is categorized as positive sequence (V_{s+}), negative sequence (V_{s-}), or zero sequence (V_{s0}).

With the negative-sequence grid voltage, along with the natural flux ψ_{sn} and forced flux (ψ_{sf}), the negative-sequence grid voltage will also inject a stator negative flux (ψ_{sne}), with a frequency of $-\omega_s$, into the system. Table .1 provides the amplitude of the negative-sequence grid voltage Vs $^-$ for various fault types. In addition to the natural and forced machines, as shown in Fig. 2(c), the negative machine is another equivalent circuit that can be used to investigate the DFIG's operation [22].

The negative machine's rotor equation is deduced as follows:

$$\left(\frac{d}{dt} - j\omega_r\right)\psi_{sne} = v_{rne} - R_r i_{rn} - \left(\frac{d}{dt} - j\omega_r\right)\sigma L_r i_{rne} \tag{8}$$

The steady-state stator-flux path following an asymmetric grid fault is an ellipse owing to the presence of forced-flux and negative sequence flux. If there is a single-phase to ground fault, the stator flux will follow a specific path as shown in Fig. 3(a).

The natural flux of the stator during an asymmetrical grid fault is affected not only by the type of fault and the level of voltage loss but also by the timing of the fault, as depicted in Fig. 3 by the 'θ' fault angle. If the fault occurs at an angle of $\theta = 90$ degrees and the positive and negative sequence grid voltages are in opposite directions, the resultant stator force and negative flux of the stator after the fault will be identical to the stator flux before the fault. As a consequence, the ψ_{sn} will be zero, as shown in Fig. 3(b). As illustrated in Fig. 3(c), the ψ_{sn} will be at its highest point when the fault occurs at the value of zero it can be expressed as

3

$$\psi_{sn}\left(t_o\right)|_{\theta=0} = \frac{2}{3}\frac{pV_s}{j\omega_s} \tag{9}$$

3. MODIFIED FUZZY LOGIC BASED PARALLEL PROTECTION SCHEME

The above rotor fault current analysis and modelling show that symmetrical and asymmetrical fault currents differ significantly. A sharp increase in rotor currents marks the beginning and end of symmetrical faults. The crowbar only needs to be turned on for a few seconds. The crowbar is ineffective for asymmetric dips because it requires the generator to be disconnected from the grid for the duration of the dip. This is explained by the fact that the magnetic flux components differ between faults [20]. As shown in Fig. 4, this section proposes a new topology of the converter protection scheme based on FL control that integrates and coordinates the REPRC, DCBC, and RSDBR protection.

3.1 CONVENTIONAL PROTECTION ARRANGEMENTS OF DFIG

The crowbar is a tool used in power electronic systems to protect against overvoltage. It creates a low resistance short circuit between terminals of rotor, triggering when an abnormal circumstance is detected. In a WEC system, it is installed on the rotor ends as shown in Fig.4 to protect against overvoltage caused by voltage dip on the grid. However, Crowbar activation causes RSPEC and wind turbines to lose control of their active and reactive powers over time. The problem with this method is that the DFIG-WEC system begins to operate as a reactive power consumption unit, such as an induction motor, resulting in grid voltage loss. The REPRC mechanism can disengage the crowbar protection and reinsert the RSPEC after a predetermined amount of time or when the rotor current and dc-link voltage return to their normal working range. To limit overvoltage, a DCBC can also be incorporated. It is a resistor connected by a switch and controlled by a hysteresis ON-OFF controller. However, it does not solve the problem of excessive rotor current.

The REPRC provides resistance in parallel with the DFIG's rotor field winding. Another method for controlling and limiting the amount of current flowing through the stator and rotor is to connect resistors in series with the DFIG windings. This study focuses on a rotor-side mounted SDBR, or RSDBR, which is connected to the rotor winding When the system is operating normally, the power electronic switch is in the closed position, and the resistor is not connected to the rotor winding when the power electronic switch is open during a fault condition. The SDBR's series architecture can manage increased rotor current and control rotor overvoltage while preventing converter control failure due to excessive voltage handled by the resistors [23]. However, the area in which it is safe to operate shrinks as the surrounding conditions deteriorate. As a result, each of these techniques has some drawbacks. A new Improved Parallel protection has been proposed to address these drawbacks.

3.2 IMPROVED COORDINATED CONTROL STRATEGY FOR FRT

The previous section covered the conventional REPRC rotor crowbar circuit. However, high currents during switching can cause torque stresses and oscillating currents on the RSPEC. This requires a high rotor voltage to manage the current, which may exceed the converter's maximum voltage capabilities and cause harm. As a result, in this section, a new approach based on fuzzy logic control is presented, which integrates and coordinates the REPRC, DCBC, and RSDBR protection, as shown in Fig. 4. The RSDBR provides primary protection in this scheme, with the crowbar circuit being activated if the RSDBR is unable to protect due to a deteriorating scenario. Depending on the situation, the REPRC will only be activated at the beginning or end of the fault. The DCBC is used to regulate the excessive voltage produced by the dc link. However, a DCBC on the DC link is not required for fault ride-through operation; however, it does help to smooth the DC link voltage and expands the normal range of DFIG operation for higher active power imbalances between the converters.

3.3 SWITCHING STRATEGY

The coordination between REPRC, DCBC, and RSDBR can be accomplished through the use of a switching mechanism designed using FL controller. It is important to note the length, kind, and position of the fault in the DFIG's fed power system to analyze the severity of the over-current during disturbances in the three-phase rotor windings of the DFIG. Some faults may cause problems with excessive current, while others may only cause problems with excessive voltage. If the protection systems are not precisely synchronized, overcurrents can damage the RSPEC's semiconductor switches and/or generate overvoltage's in the DC link capacitor.

This paragraph describes the protection mechanism for a DFIG system in the event of faults. Table 2 shows scenarios for over-current and over-voltage problems, with the most vulnerable component of the DFIG identified in the third column, and the protection system that should be activated in the fourth column. If the first protective mechanism fails, the second system attempts to minimize the excess current or voltage, and if it still exceeds the maximum permissible value, the DFIG PECs are disconnected, according to the final column in Table 2. Fuzzy logic (FL) is used to design the protection mechanism, with the Sugeno FL model suggested using MATLAB-Simulink, as it requires fewer hardware resources than standard Boolean logic. Fig. 4 shows the proposed mechanism using FL.

The protection system for converters is designed using fuzzy if-then rules as discussed in Table 2 with two input variables: rotor current and DC bus voltage. Each variable has a defined range with membership functions. The rules generate three output

variables to determine if the protection system should be turned on or off. The following are the inputs:

- Rotor current
- DC Link Voltage

The first input's Membership function (MF) is defined as follows:

- LOW
- MEDIUM
- HIGH
- NEGATIVEMID
- NEGATIVEHIGH

The first MF 'LOW' is placed in the acceptance limits that it does not destabilize the system. The second MF 'MEDIUM' is positioned in the system such that its current value is between the rated current and the current that can cause system damage. The third MF 'HIGH' has the current through the circuit is extremely high and has the potential to cause system damage. Similarly for the negative values membership functions is designed.

Similarly in the second input the Membership function is defined as follows

- LOW
- MEDIUM
- HIGH

The first membership function 'LESS' is placed in the acceptance limits so that it does not destabilize the system. The second membership function 'HIGH' is positioned in the system such that its voltage value is between the rated voltage and the voltage that can cause system damage. The third membership function 'VERY HIGH' has a voltage through the circuit that is extremely high and has the potential to cause system damage.

Three different outputs are used to map the different inputs of the membership function. They are as follows:

- RSDBR ON
- DCBC ON
- CROWBAR ON

This study uses the Takagi-Sugeno-Kang technique of fuzzy inference to identify the output, the only difference between it and mamdani is that the sugeno output function is either linear or constant, and in this study, the constant output membership function is used called as fuzzy singleton. A fuzzy singleton, is a fuzzy set with a membership function which is unity at one point in the universe and zero everywhere else. The basic conditions of the Sugeno fuzzy inference system are as follows:

If Input= p and Input 2 = q, then Output is z =f (p, q)

Usually f (p, q) is a polynomial of the input variables p and q. but it can be any function. In this model 'f' is constant ($z=pa+qb+c$ where (a=b=0) because of a fuzzy singleton case).

The output level z_i of each rule is weighted by the firing strength w_i of the rule. For example, for an AND rule with Input 1 = p and Input 2 = q, the firing strength is

$$w_i = AND\ Method\ (F1(p),\ F2(q))$$

Where *F1(p), F2(q)* are the membership functions for Inputs 1 and 2. The weighted mean of all rule responses, calculated as the final output of the system.

$$Final\ Output\ = \frac{\sum_{i=1}^{N} w_i z_i}{\sum_{i=1}^{N} w_i}$$

Where N is the number of rules.

For the first output variable, two membership functions are used to toggle the RSDBR protection SMALL and LARGE. Whereas SMALL defines Off state and LARGE denotes ON state. Similarly, the membership functions for the second and third outputs are SMALL and LARGE, the second output is used for CHOPPER switching, and the third output is used for CROWBAR. The following are the membership functions:

- SMALL
- LARGE

Lastly, the input membership functions and the output membership functions are plotted using well-defined sets of rules. If-then rules are used to set the following rules.

3.4 RSDBR AND REPRC RESISTANCE VALUES

The correct value of the resistance is usually the most crucial aspect in reducing the rotor current. It is not enough to determine the resistance value based only on the lower rotor current that occurs under fault conditions. Under faults, this selected value

should be subject to a minimal DC voltage tolerance variation. It is important to select appropriate values for the resistor parameters. The RSDBR and REPRC resistance values can be determined from a transient study of stator voltage magnitude fluctuations, slip, and rotor speed. The resistance values are calculated under the worst conditions (with the highest peak current): Symmetric voltage drops up to 1.0p.u in the most severe condition. The expressions of the rotor-current are derived below:

As can be seen from Equation (1-4), RSPEC is a way to regulate the rotor voltage (v_r), which in turn is used to control the DFIG. First, remove i_s from Equation (3) and (4), then sustitute it into Equation (2). then, eliminate rotor flux ($\overrightarrow{\psi_r}$), which leads to the formula.

$$\overrightarrow{v_r} = \frac{L_m}{L_s}\left(\frac{d}{dt} - j\omega_r\right)\overrightarrow{\psi_r} + [R_r + \left(\frac{L_s L_r - L_m^2}{L_s}\right)\left(\frac{d}{dt} - j\omega_r\right)]\overrightarrow{i_r} \tag{10}$$

Defining leakage factor as

$$\lambda = \frac{L_s L_r - L_m^2}{L_s} \tag{11}$$

The voltage produced by the stator flux is then represented by a voltage source $\overrightarrow{v_{ro}}$

$$\overrightarrow{v_{ro}} = \frac{L_m}{L_s}\left(\frac{d}{dt} - j\omega_r\right)\overrightarrow{\psi_r} \tag{12}$$

So Equation (10) becomes

$$\overrightarrow{v_r} = \overrightarrow{v_{ro}} + [R_r + \lambda\left(\frac{d}{dt} - j\omega_r\right)]\overrightarrow{i_r} \tag{13}$$

In Equation (13), It is useful to interpret the rotor voltage in the rotor reference frame by multiplying both sides by $e^{-j\omega rt}$)

$$\overrightarrow{v_r^r} = \overrightarrow{v_{ro}^r} + R_r\overrightarrow{i_r^r} + \lambda L_r \frac{d\overrightarrow{i_r^r}}{dt} \tag{14}$$

This Equation describes the connection between rotor voltage and current. As a result, the rotor circuit model is obtained and illustrated in Fig. 5 with all earlier protection systems.

The voltage expression for phase 'a' is

$$v_{ra}(t) = Re\{\overrightarrow{v_{ro}^r}\} + R_r i_{ra}(t) + \lambda L_r \frac{d\overrightarrow{i_{ra}^r}(t)}{dt} \tag{15}$$

For $i_{ra}(t)$ can be expressed in the form of a linear differential equation

$$i_{ra}'(t) + \frac{R_r}{\lambda L_r}i_{ra} = \frac{1}{\lambda L_r}[v_{ra}(t) - Re\{\overrightarrow{v_{ro}^r}\}] \tag{16}$$

Consequently, with the converter operational, $v_{ra}(t) = V_r cos(s\omega_s t + \beta)$, where β is the phase-a rotor voltage angle at the time of loss.

For a symmetrical voltage interruption on the stator, if there will be a three-phase step magnitude transition from V_s to $(1-p) V_s$ (where p is the voltage sag ratio), $\overrightarrow{v_{ro}^r}$ in Equation (14) can surpass the upper limit voltage that the RSPEC can produce, causing the current control to fail. The voltage is [24]

$$\overrightarrow{v_{ro}^r} = (1-p)V_s\frac{L_m}{L_s}se^{js\omega_s t} - \frac{L_m}{L_s}(\frac{1}{\tau_s} + j\omega_r)\frac{pV_s}{j\omega_s}e^{-1/T_s} \tag{17}$$

Considering that time constants are defined as

$$T_r = \frac{\lambda L_r}{R_r}, \ T_s = \frac{L_s}{R_s}, \ T = \frac{T_s T_r}{T_s - T_r} \tag{18}$$

Equation (17) can be modified by discarding $1/T_s$, which is negligible due to the minimal stator resistance of the generator; hence, $1/T_s$ can be omitted.

$$\overrightarrow{v_{ro}^{r}} \approx V_{s}\frac{L_{m}}{L_{s}}[s(1-p)se^{js\omega_{s}t}-(1-s)pe^{-j\omega_{r}t}e^{-t/T_{s}}]$$ (19)

From Equation (16) and (19), the final expression of $i_{ra}(t)$ can be solved and split into four parts.

$$\dot{i}_{ra}(t)=\dot{i}_{dc}+\dot{i}_{vr}+\dot{i}_{vrn}+\dot{i}_{vrf}$$ (20)

Where the components are

$$i_{dc}=i_{r\alpha}\left(t_{0}^{-}\right)-\frac{1}{\lambda L_{r}}\frac{T_{r}}{1+T_{r}^{2}(s\omega_{s})^{2}}\times[V_{r}\cos\beta-V_{s}\frac{L_{m}}{L_{s}}s(1-p)]-\frac{1}{\sigma L_{r}}V_{s}\frac{L_{m}}{L_{s}}(1-s)\,p\frac{T}{1+T^{2}(\omega_{r})^{2}}e^{\frac{-t}{T_{r}}}$$ (21)

$$i_{vr}=\frac{V_{r}}{\lambda L_{r}}[\frac{T_{r}}{1+T_{r}^{2}(\omega_{r})^{2}}cos(s\omega_{s}t+\beta)+\frac{T_{r}^{2}}{1+T_{r}^{2}(\omega_{r})^{2}}sin(s\omega_{s}t+\beta)]$$ (22)

$$i_{vrf}=\frac{1}{\lambda L_{r}}V_{s}\frac{L_{m}}{L_{s}}s(1-p)\times[\frac{T_{r}}{1+T_{r}^{2}(s\omega_{s})^{2}}cos(s\omega_{s}t)+\frac{T_{r}s\omega_{s}}{1+T_{r}^{2}(s\omega_{s})^{2}}sin(s\omega_{s}t)]$$ (23)

$$i_{vrn}=\frac{V_{s}}{\lambda L_{r}}\frac{L_{m}}{L_{s}}s(1-p)\times[\frac{T}{1+T^{2}\omega_{r}^{2}}cos(\omega_{r}t)+\frac{T^{2}\omega_{r}}{1+T^{2}(\omega_{r})^{2}}sin(\omega_{r}t)]e^{\frac{-t}{T_{s}}}$$ (24)

Due to the lower stator resistance, the relevant approximations are made: $e^{-t/T_{s}}\approx 1;T=T_{r}$. The components of the current are then written as a single trigonometric function as a

$$i_{dc}=i_{ra}\left(t_{0}^{-}\right)-\frac{1}{\lambda L_{r}}\frac{T_{r}}{1+T_{r}^{2}(s\omega_{s})^{2}}\times V_{r}cos\beta-\frac{1}{\lambda L_{r}}V_{s}\frac{L_{m}}{L_{s}}(1-s)\,p\frac{T}{1+T^{2}(\omega_{r})^{2}}e^{\frac{-t}{T_{r}}}$$ (25)

$$i_{vr}=\frac{V_{r}}{\lambda L_{r}}[\frac{T_{r}}{\sqrt{1+T_{r}^{2}(\omega_{r})^{2}}}sin(s\omega_{s}t+\beta+\delta)]$$ (26)

$$i_{vrf}=0$$ (27)

$$i_{vrn}=\frac{V_{s}}{\lambda L_{r}}\frac{L_{m}}{L_{s}}(1-s)\times[\frac{T_{r}}{\sqrt{1+T_{r}^{2}\omega_{r}^{2}}}sin(\omega_{r}t+\delta)$$ (28)

Taking each component's amplitude at its maximum current value into consideration

$$i_{r\alpha,max}=i_{r\alpha}(t_{0}^{-})-\frac{V_{s}}{\lambda L_{r}}\frac{L_{m}}{L_{s}}(1-s)\frac{T_{r}}{1+T_{r}^{2}(\omega_{r})^{2}}+\frac{V_{r}}{\lambda L_{r}}\frac{T_{r}}{\sqrt{1+T_{r}^{2}(\omega_{r})^{2}}}+\frac{V_{s}}{\lambda L_{r}}\frac{L_{m}}{L_{s}}(1-s)\frac{T_{r}}{\sqrt{1+T_{r}^{2}\omega_{r}^{2}}}$$ (29)

In addition to this, the boundary conditions are

$$i_{r\alpha,max}\leq I_{th\_RSDBR},\qquad V_{r}\leq V_{th\_RSPEC.}$$ (30)

As a result, (29) and (30) are Equation that T_{r} can be solved.

With the protective mechanisms

$$T_{r}=\frac{\lambda L_{r}}{R_{r}+R_{protection}}$$ (31)

Finally, the crucial resistance value known as $R_{protection}$ can be determined. If the rotor fault currents are unable to be effectively restricted, the crowbar can be utilized as supplemental protection. $R_{protection}$ refers to total resistance, which comprises RSDBR and REPRC. RSDBRs provide current-limiting operation, so the critical condition for the crowbar resistance is the voltage across it must be within the limits of the rotor voltage to which it is connected in parallel: $R_{CB}\times i_{r,max}\leq V_{r,max}$. As a result, crowbar resistance contributes only a minor portion of total $R_{protection}$. This method of resistors with minimum and maximum levels is easier to use than crowbar protection alone. The rotor winding current limit sets the lowest value, and the converter terminal voltage limit sets the highest [24].

4. SIMULATION RESULTS

In MATLAB Sim-Power Simulink, a WEC system with six 1.5 MW DFIG-based wind turbines tied to a 25 kV distribution structure that transmits power to a 120 kV grid via a 30-km 25 kV feeder was modeled. The system was tested for dynamic

response under various faults at "0.5 s". The system was initially tested without any protection, then with REPRC, and finally with the proposed coordinated protection scheme. The simulation time was kept short to check the system's rapid response. The findings are analyzed in the subsequent subsections. The appendix provides the generator parameters. The simulation was conducted with a constant wind speed of 15 m/s and the DFIG WEC system supplying real power to the power system. The simulated fault condition is:

1)A symmetrical three-phase LLLG fault for 0.2 seconds
2) An Asymmetrical LL fault on two phases for 0.2 seconds
3) A Two phase to ground Asymmetrical LLG fault for 0.2 seconds

The values for the thresholds that are used in the calculation of R_{RSDBR} and R_{REPRC} are as follows: I_{th} RSDBR = 1.5 p.u., and I_{th} REPRC = 1.8 p.u. rotor slip is s= -0.2 p.u. for before the faults.

From Equation (30) and (31), τ_r = 0.26584 p.u., $R_{protection}$ = 1.21 p.u. = 0.4719 Ω. In summary, the total value of protection resistance should be 0.4719 ohm, and the task now is to find the optimal resistance value for the RSDBR in the DFIG system. This is important for maintaining LVRT capability, but increasing resistance can impact system efficiency and increase losses. The optimal value will be determined through MATLAB simulation during a 3-phase fault. In the system if the rotor fault currents cannot limit effectively, then only crowbar can be used as further protection. The total resistance is $R_{protection}$, includes RSDBR and REPRC. The current-limiting function is provided by the RSDBR, hence the critical criterion of crowbar resistance is that the voltage across it must be within the rotor voltage limit, for its shunt connection: $REPRC \times i_{r,max} \leq V_{r,max}$. Therefore, the crowbar resistance is a small contribution to the total $R_{protection}$. This is simpler than using crowbar protection alone, where the resistance has a lower and upper limit. The minimum value is restricted by the rotor winding current limit, while the maximum is set by the voltage limit.

To find the optimal value of resistance of RSDBR protection the additional simulation is conducted to investigate the impact of varying the RSDBR resistance on the LVRT capability of the system which is shown below in the form of graphs in the Fig.6 and it shows that the optimum value for the RSDBR is 0.4ohm because the peak of stator, rotor current and DC Link voltage is minimum in the case of using 0.4 ohm and similarly the torque oscillation is minimum in the case of 0.4 ohm

Then, the selected resistance values are R_{RSDBR} = 0.4 Ω, R_{REPRC} = 0.0719 Ω. Based on monitoring the maximum magnitude of dc voltage during the fault, the DCBC is activated. The relation between the charging activity and DCBC can be expressed as follows:

$$V_{r,max} - IR_{DCBC} - V_{DC} = 0 \tag{32}$$

According to Equation (32), it is possible to estimate the value of the DCBC " R_{DCBC} by assuming that, in the event of a fault, the source voltage is zero (" $V_{r,\,max}$ = 0"). In this case, the current "I" through the resistor drops as the capacitor's loss of charge causes the voltage to drop. Upon reaching the nominal value of the capacitor's voltage, the dc-link crowbar resistance is determined, Therefore R_{DCBC} is taken as 0.5 ohm.

4.1 SYMMETRICAL FAULT CONDITION

The simulation results from Fig 7-9 demonstrate the response of a DFIG during a LLLG symmetrical fault. Prior to the fault occurrence, the grid voltage and stator voltage remain constant, and the DFIG operates under normal conditions. The stator current and rotor current waveforms exhibit excellent performance, while the DC-link voltage remains constant, and the reactive power is maintained at nearly zero VAR. However, at time t=0.5 seconds, the grid fault instantaneously reduces the output voltage of the wind generator and decreases the stator voltage to 10% of its original value as can be seen in the Fig. 7. This results in an abrupt increase in the rotor and stator current up to 4p.u, as well as an overvoltage in the DC-link bus voltage as shown in Fig. 7. Without the protection system, the DFIG is unable to achieve fault ride-through (FRT) and can cause damage to the system's equipment due to the large failure voltages and currents.

A traditional protection technique REPRC is used to protect a grid-connected DFIG-based system. This technique, however, has a disadvantage, its excitation causes the RSPEC and WT to lose control over their ability to control active and reactive power over the time. The REPRC technique is configured to activate whenever the rotor current exceeds 1.5 times the rated current; at this point, the RSPEC is short-circuited. The system detects stator-voltage losses at time t=0.5 seconds, triggering the REPRC and stopping the RSPEC. Fig. 8 depicts the REPRC resistor current's behaviour, which rapidly increases and then rapidly decreases over time. This traditional protection technique has a substantial inhibiting effect on fault currents in the rotor and stator, limiting them within the DFIG system's permissible limits. Fig. 8 also shows that with REPRC protection, the DC-link voltage drops significantly, especially when compared to Fig. 7. Although this traditional protection technique is effective in preventing system damage, its impact on active and reactive power control must be carefully considered.

Fig. 9 depicts the switching of the Improved Parallel coordinated protection scheme, which shows that the RSDBR is engaged seven times to ensure that the rotor current is not exceeded. If the rotor current exceeds the REPRC threshold, the REPRC activates four times with the RSDBR engaged, while the DC Chopper protection is activated twice to ensure that the DC link voltage is within acceptable limits. According to the specifications, the improved parallel protection system method can

4

effectively suppress the rotor current in less than 2 pu, implying that the FRT performance is superior to both no protection and REPRC protection, as shown in Fig. 9. When using a REPRC alone, the DC-link voltage takes longer to reach a steady voltage level. When the parallel improved protection technique is used concurrently, this phenomenon is not observed. Even if the REPRC is only engaged for a brief period of time, the voltage on the dc connection becomes stable, and the dc-link voltage variation range is reduced to "30 V" with the parallel improved control protection technique, as illustrated in Fig. 9. As a result, it is clear that the DCBC must be used in conjunction with the RSDBR and REPRC. This integration may aid in reducing the dc voltage swings that occur during a fault in a more efficient manner, thereby reducing the REPRC switching time. As a result, DFIG will not function as a SEIG for an extended period of time, resulting in the generator losing control in a relatively short period of time. As a result, when attempting to control its reactive energy exchange with the grid, the machine will have a faster response time. The simulation results in Fig.9 demonstrate the effectiveness of the improved method by limiting stator current and reducing dc bus voltage fluctuation to less than 1.2 times the rated value, ensuring that the converter is not affected. The comparative performance analysis is depicted in detail in Fig. 10.

4.2 Asymmetrical Fault Condition

The functioning of the proposed coordinated technique in an asymmetrical fault condition is shown in this section. This section demonstrates the operation of the proposed coordination method under asymmetric fault conditions. The results obtained when using the modified coordinated protection strategy are included in this part of the paper and also in the absence of a protection system. The waveforms illustrated in Fig.11-12 represent the simulated results of a two-phase short-circuit fault occurring in the power system. These results show the voltage dropping to fifty percent without any protection technique, as well as with protection techniques. In addition, Fig.13 displays a comparison of peak values for voltage and current during faults with and without protection. Moving on, Fig.14-15 illustrate the waveforms that are generated in the event of a two-phase-to-ground short-circuit fault occurring, resulting in the grid voltage dropping to fifty percent. Wind energy collected by wind turbines does not change significantly, resulting in an increase in the turbine's speed. A 2-phase short circuit and 2-phase grounding fault cause a short-term speed fall, signifying that the speed of the rotor is lesser than its synchronous speed at this moment. When the speed falls, the GSPEC is in the rectifier state; as the speed increases, the GSPEC shifts to the inverter state. The current of the rotor rises as the speed rises because the slip power increase through the RSPEC as shown in Fig. 11 and 13 Fig. 11-15 demonstrates that, prior to the occurrence of the fault, the grid voltage and stator voltage both remained constant, the DFIG is functioning normally, the waveforms of the stator current and rotor current are quite excellent, and the voltage of the DC-link voltage is also sustained constant and the reactive power has been almost maintained at 0 VAR. After the fault, the negative-sequence part of the stator flux linkage produces a surge current in the rotor current. In addition, stator current increased quickly up to 4p.u; the DC-link bus voltage also illustrates over-voltage as can be seen in the Figures of the absence of protection technique which is Fig. 11 and 14. At time t = 0.5s, the Modified configuration recognizes the stator voltage loss and rise in rotor current and DC link bus voltage thus activating the protection system with the help of fuzzy logic control without stopping the RSPEC. The RSDBR has the distinctive advantage of being able to control the current directly. Furthermore, because the RSDBR is configured in series, the high voltage is shared by the resistance, so the induced excessive voltage does not cause RSPEC control to fail, and it also limits excessive rotor current. The modified control method can suppress the current and voltage surge, as shown in Fig. 12-15. The Modified FL-based technique in this paper improves rotor current suppression during faults, and with the help of a FL-based controller, a wide range of conclusive results can be obtained as shown in Fig. 13 & 16, and since the FL technique requires less hardware than traditional boolean values it is found to be acceptable and advantageous to use this technique.

5. RTS RESULTS DISCUSSION

A case study was conducted in this section using a real-time simulator (RTS) to strengthen the credibility of antecedent analysis. RTS is a computer-based system that allows engineers to simulate complex scenarios, observe system behavior, and test the effectiveness of protection and control schemes in real-time. With the advancement of hardware and software technologies, RTS has become an essential tool for power system analysis, power electronics, control system design, and renewable energy systems. In this context, this paper discusses the use of an RTS tool (OP4500) for simulating the behavior of a power system with a DFIG-based wind generator, with and without protection systems. The platform incorporates FL-based techniques and employs a range of components, including a host PC, DB-37 connector, BNC cables, HIL system, and GWinstek GDS-1104B DSO as depicted in Fig. 17. It is important to note that all parameters were expressed in per-unit form and assigned a multiplication factor of one.

The results of a symmetrical voltage dip in a 1.5 MW DFIG WEC system without any protective measures are demonstrated in Fig. 18. In the event of a minor disturbance at 0.5s, the grid voltage plummets to 0.2pu, as evident from the graph. At t = 0.5s, the grid failure instantaneously reduces the output voltage of the wind generator, along with a drop in the stator voltage to 10% of its current value, which is depicted in Fig. 18(a). Furthermore, the stator and rotor currents exhibited a rapid increase, and the DC-link bus indicated over-voltage, as shown in Fig. 18(c).

Now a modified FL based coordinated protection technology is used as the protection unit. The RTS result with modified

strategy shown in Fig.19-22 for both the Asymmetrical and Symmetrical faults shows that for the entire fault time, the peak rotor and stator current never surpassed the estimated maximum limit of 2 p.u. Modified configuration detects a sudden rise in rotor current and Dc Link bus voltage and activates the security mechanism with the help of the FL tool without interfering with the RSPEC. The Modified technique demonstrated remarkable efficacy in curbing the stator and rotor's three-phase current within the permissible limit of 2 pu, as illustrated in Fig. 19-22. In addition, the modified methodology obliterates the substantial torque fluctuations linked with fault activation, as evidenced by the simulation and RTS outcomes. Furthermore, the modified technique manifests its potential to mitigate the PEC's potential harm by ensuring stator current regulation and containing dc-bus voltage fluctuations to a maximum of 1.5 times the rated value.

6. CONCLUSION

The proposed technique Fuzzy Logic Controlled Parallel Protection has proven to be effective in enhancing the Fault Ride Through (FRT) capability of the DFIG system. The technique has shown its ability to limit the peak values of fault rotor current, stator current, and dc-link voltage while protecting the rotor-side converter, avoiding frequent use of crowbar short-circuit, and extending RSPEC operation time. The presented current expressions and resistance calculations for the RSDBR and the crowbar provide valuable insights into the design of the protection strategy. The validation of the proposed protection technique using MATLAB simulation and OPAL-RT has demonstrated effectiveness in both symmetrical and asymmetrical fault scenarios. This technique can be implemented in real-time to ensure the smooth operation of DFIG systems during grid faults. Overall, the proposed technique has the potential to improve the reliability and stability of the DFIG system, thereby contributing to the efficient utilization of renewable energy sources.

7. STATEMENTS AND DECLARATIONS

8. REFRENCES

[1] "Global Wind Report 2021 - Global Wind Energy Council", https://gwec.net/global-wind-report-2021/.

[2] Vali, A. A., Hosseini, S. M. H., and Olamaei, J., "Control of doubly-fed induction generator with extended state observer under unbalanced grid conditions", *Scientia Iranica*, **29**(5), pp. 2498–2514 (2022). doi: 10.24200/SCI.2020.55054.4054

[3] Ansari, A. A. and Dyanamina, G., "MATLAB Simulation of FRT Techniques for DFIG-based Wind Farms", *2021 International Conference on Control, Automation, Power and Signal Processing (CAPS)*, pp. 1–6. IEEE, (2021). doi: 10.1109/CAPS52117.2021.9730674.

[4] Ansari, A. A. and Dyanamina, G., "Fault Ride-Through Operation Analysis of Doubly Fed Induction Generator-Based Wind Energy Conversion Systems: A Comparative Review", *Energies*, **15**(21), p. 8026 (2022). https://doi.org/10.3390/en15218026

[5] Mahela, O. P., Gupta, N., Khosravy, M., and Patel, N., "Comprehensive overview of low voltage ride through methods of grid integrated wind generator", *IEEE Access*, **7**, pp. 99299–99326 (2019). doi: 10.1109/ACCESS.2019.2930413.

[6] Haidar, A. M. A., Muttaqi, K. M., and Hagh, M. T., "A coordinated control approach for DC link and rotor crowbars to improve fault ride-through of dfig-based wind turbine", *IEEE Trans Ind Appl*, **53**(4), pp. 4073–4086 (2017). doi: 10.1109/TIA.2017.2686341.

[7] Huang, J., Zhang, L., Sang, S., et al., "Optimized Series Dynamic Braking Resistor for LVRT of Doubly-Fed Induction Generator With Uncertain Fault Scenarios", *IEEE Access*, **10**, pp. 22533–22546 (2022). doi: 10.1109/ACCESS.2022.3154042.

[8] Du, K., Ma, X., Zheng, Z., Li, C., et al., "LVRT Capability Improvement of DFIG-Based Wind Turbines with a Modified Bridge-Resistive-Type SFCL", *IEEE Transactions on Applied Superconductivity*, **31**(8), pp. 1-5 (2021). doi: 10.1109/TASC.2021.3091114.

[9] Asghar, R., Rehman, F., Ullah, Z., et al., "Modified switch type fault current limiter for low-voltage ride-through enhancement and reactive power support of DFIG-WT under grid faults", *IET Renewable Power Generation*, **14**(9), pp. 1481–1490 (2020). https://doi.org/10.1049/iet-rpg.2019.1058

[10] Puchalapalli, S. and Singh, B., "A Novel Control Scheme for Wind Turbine Driven DFIG Interfaced to Utility Grid", *IEEE Trans Ind Appl*, **56**(3), pp. 2925–2937 (2020). doi: 10.1109/TIA.2020.2969400.

[11] Sahoo, S. S., Chatterjee, K., and Tripathi, P. M., "A coordinated control strategy using supercapacitor energy storage and series dynamic resistor for enhancement of fault ride-through of doubly fed induction generator", **16**(8), pp. 615–626 (2019). https://doi.org/10.1080/15435075.2019.1602531,

[12] Gayathri, N. S. and Senroy, N., "Wind turbine with flywheel for improved power smoothening and LVRT", *IEEE Power and Energy Society General Meeting*, Vancouver, BC, Canada, pp. 1-5, doi: 10.1109/PESMG.2013.6672812. (2013).

[13] Shiddiq Yunus, A. M., Abu-Siada, A., Mosaad, M. I., et al., "Application of SMES Technology in Improving the Performance of a DFIG-WECS Connected to a Weak Grid", *IEEE Access*, **9**, pp. 124541–124548 (2021). doi: 10.1109/ACCESS.2021.3110995.

[14] Thet, A. K. and Saitoh, H., "Pitch control for improving the low-voltage ride-through of wind farm", *Transmission and Distribution Conference and Exposition: Asia and Pacific, T and D Asia,* pp. 1-4 Seoul, Korea (South)(2009). doi: 10.1109/TD-ASIA.2009.5356993.

[15] Choopani, M., Hosseinian, S. H., and Vahidi, B., "New Transient Stability and LVRT Improvement of Multi-VSG Grids Using the Frequency of the Center of Inertia", *IEEE Transactions on Power Systems*, **35**(1), pp. 527–538 (2020). doi: 10.1109/TPWRS.2019.2928319

[16] Bounar, N., Labdai, S., Boulkroune, et al., "Adaptive Fuzzy Control Scheme for Variable-Speed Wind Turbines Based on a Doubly-Fed Induction Generator", *Iranian Journal of Science and Technology - Transactions of Electrical Engineering*, **44**(2), pp. 629–641 (2020). https://doi.org/10.1007/s40998-019-00276-6

[17] Liang, J., Howard, D. F., Restrepo, et al., "Feedforward transient compensation control for DFIG wind turbines during both balanced and unbalanced grid disturbances", *IEEE Trans Ind Appl*, **49**(3), pp. 1452–1463 (2013). doi: 10.1109/TIA.2013.2253439.

[18] Abazari, S. and Dehkordi, S. F., "Sliding-Mode Control for a DFIG-Based Wind-Power Generation System with Series Grid-Side Converter under Unbalanced Grid Voltage Conditions", *Scientia Iranica*, **25**(3), pp. 1507–1522 (2018). doi: 10.24200/SCI.2017.4367

[19] Sguarezi Filho, A. J., "Fundamentals of vector control for DFIG and for the three-phase CCG", In *Model Predictive Control for Doubly-Fed Induction Generators and Three-Phase Power Converters*, pp. 27-41 Elsevier (2022). https://doi.org/10.1016/B978-0-32-390964-8.00012-9

[20] Abad, G., López, J., Rodríguez, M. et al., "Dynamic Modeling of the Doubly Fed Induction Machine", In *Doubly Fed Induction Machine: Modeling and Control for Wind Energy Generation Applications,* IEEE, pp.209-239 (2011), doi: 10.1002/9781118104965.ch4.

[21] López, J., Sanchis, P., Roboam, X., and Marroyo, L., "Dynamic behavior of the doubly fed induction generator during three-phase voltage dips", *IEEE Transactions on Energy Conversion*, **22**(3), pp. 709–717 (2007). doi: 10.1109/TEC.2006.878241.

[22] López, J., Gubía, E., Sanchis, P., et al., "Wind turbines based on doubly fed induction generator under asymmetrical voltage dips", *IEEE Transactions on Energy Conversion*, **23**(1), pp. 321–330 (2008). doi: 10.1109/TEC.2007.914317.

[23] Causebrook, A., Atkinson, D. J., and Jack, A. G., "Fault ride-through of large wind farms using series dynamic braking resistors (March 2007)", *IEEE Transactions on Power Systems*, **22**(3), pp. 966–975 (2007). doi: 10.1109/TPWRS.2007.901658.

[24] Morren, J. and de Haan, S. W. H., "Short-circuit current of wind turbines with doubly fed induction generator", *IEEE Transactions on Energy Conversion*, **22**(1), pp. 174–180 (2007). doi: 10.1109/TEC.2006.889615.

9. APPENDIX

Variables	Value Implemented
Power	6×1.5 MW
Stator Nominal voltage (V_{rms})	575 V
Rotor Nominal voltage (V_{rms})	1975 V
Frequency	60 Hz
Resistance of Stator	0.023 p.u
Inductance of Stator	0.18 p.u
Resistance of Rotor	0.016 p.u
Inductance of Rotor	0.16 p.u
Mutual inductance	2.9 p.u
Pairs of Pole	3

AFTAB AHMED ANSARI is a dedicated researcher and a Student Member of the IEEE. He completed his B.E. degree in Electrical and Electronics Engineering from Rajiv Gandhi Proudyogiki Vishwavidyalaya (RGPV) Bhopal, Madhya Pradesh, India in 2017. Subsequently, he obtained his M.E. degree in Power System from the University Institute of Technology RGPV (UIT-RGPV) Bhopal, India in 2019. Currently, he is a Research Scholar in the Electrical Engineering Department at Maulana Azad National Institute of Technology Bhopal (MANIT-B), India. AFTAB's research interests span various fields including DFIG based wind energy system, grid fault ride through, Multi-Level Inverters, AI, and Renewable Energy Sources.

DR. GIRIBABU DYANAMINA (Senior Member, IEEE) received a B.Tech. degree in electrical and electronics engineering from Jawaharlal Nehru Technological University (JNTU), Hyderabad, Telangana, India in 2006, and his M.T. degree in power electronics from JNTU in 2008, and Ph.D degree in electrical engineering in the Indian Institute of Technology Roorkee (IITR), Uttarakhand, India. In 2013, he joined the National Institute of Technology Kurukshetra (NIT-KKR), Haryana, India, as an Assistant professor in the Electrical Engineering Department. In 2019, he joined the Maulana Azad National Institute of Technology Bhopal (MANIT-B), India, the Electrical Engineering Department, where he works as an assistant professor. He is a senior IEEE member. His research interests include sensorless speed control of electric drives, multi-level inverters, AI, and renewable energy sources.

Figure Content

Fig 1 DFIG's stators' flux paths during symmetrical voltage sags (a) prior to sag (b) during sag (c) after sag
Fig 2 DFIG equivalent circuit model exposed to symmetrical voltage sag: (a) natural-machine and (b) forced-machine (c) negative machine
Fig 3 Flux path of the stator in the event of an asymmetrical grid failure (a) Steady-state after a fault (b) the zero flux state; and (c) the maximum natural flux state.
Fig 4 DFIG with Modified FL-based parallel protection scheme
Fig 5 Model of DFIG rotor equivalent circuit illustrating all protection schemes
Fig 6 Optimal value of resistance of RSDBR for protection
Fig 7 DFIG's dynamic behavior in the absence of a protection system with Symmetrical Fault
Fig 8 DFIG's dynamic behavior in the presence of Crowbar protection system with Symmetrical Fault
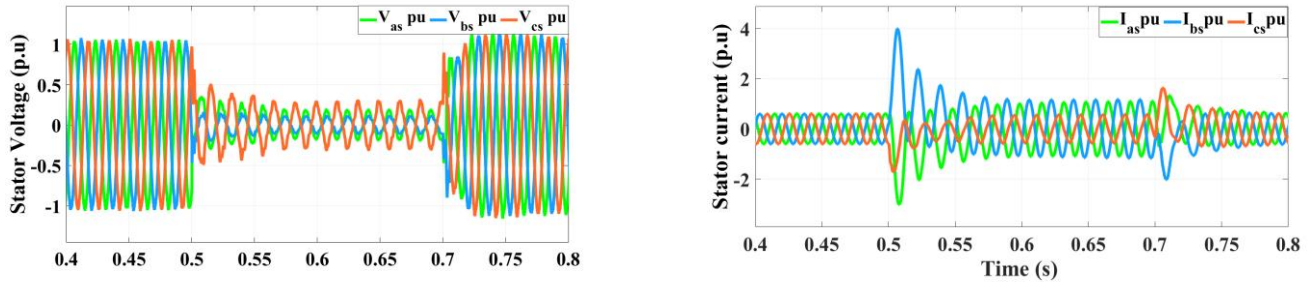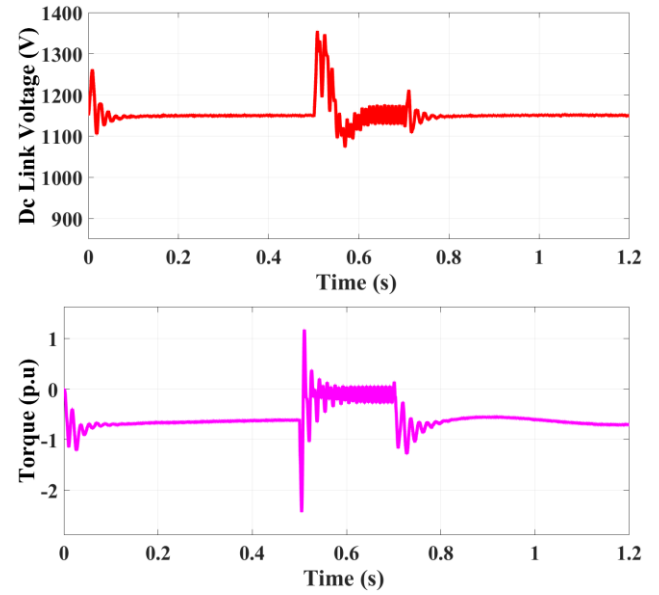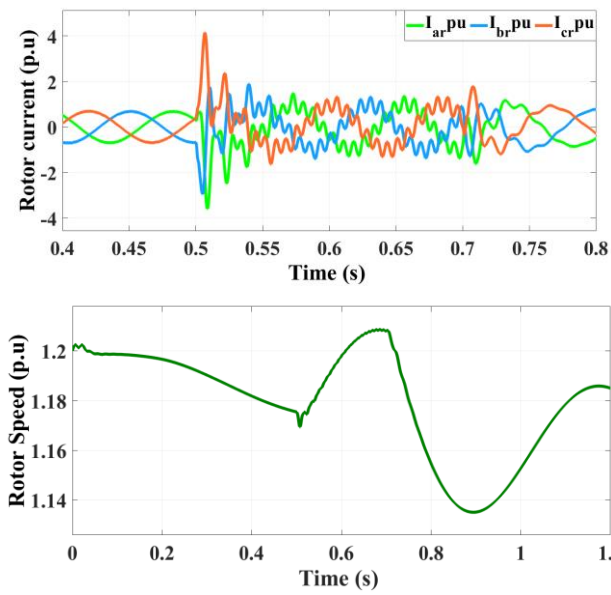**Fig 9** DFIG's dynamic behavior in the presence of Proposed protection system with Symmetrical Fault
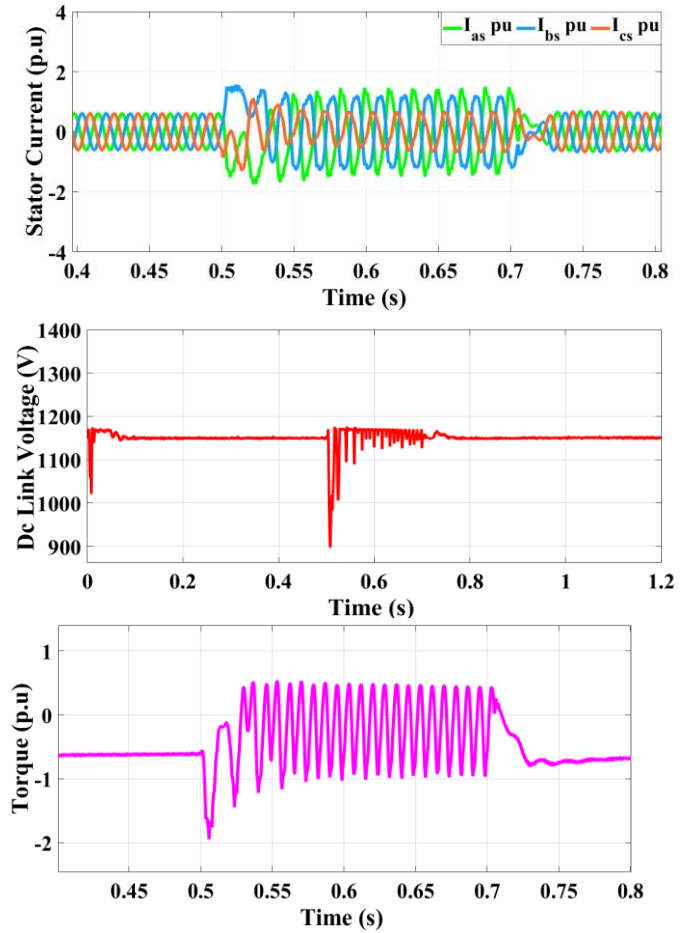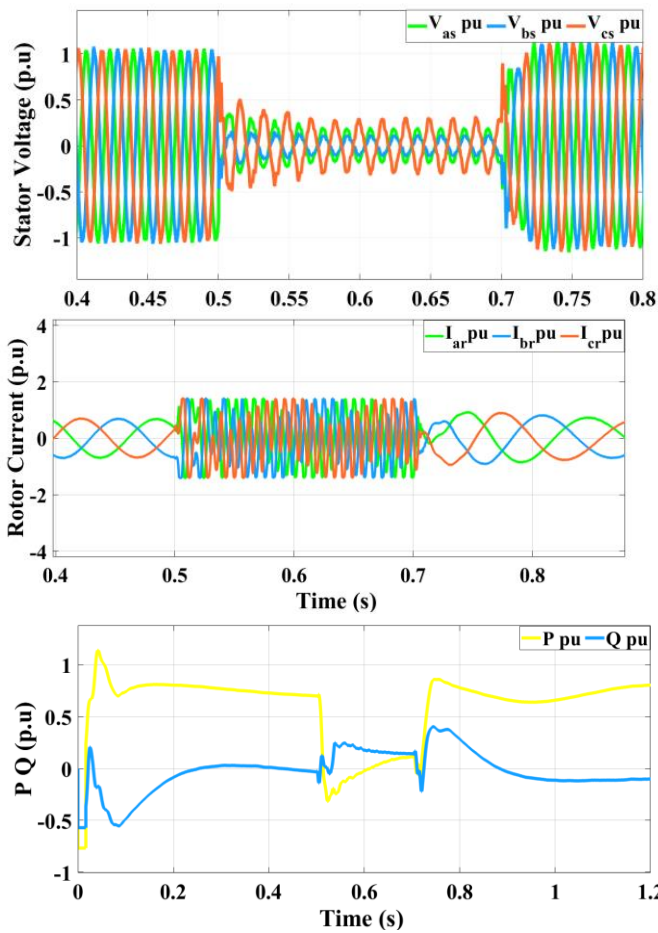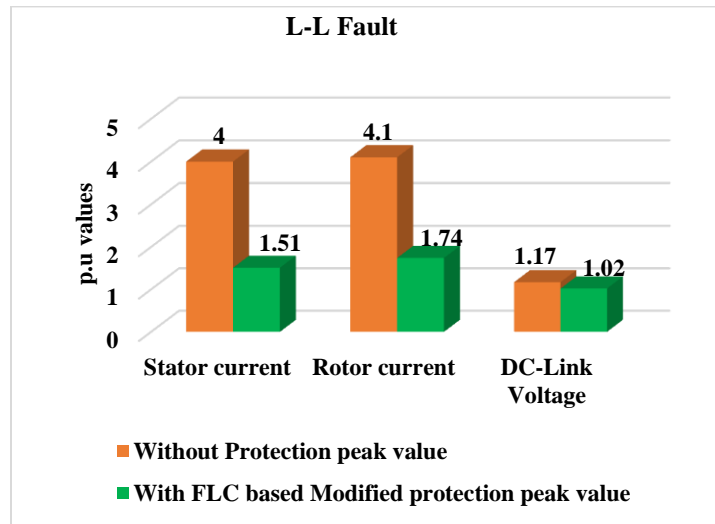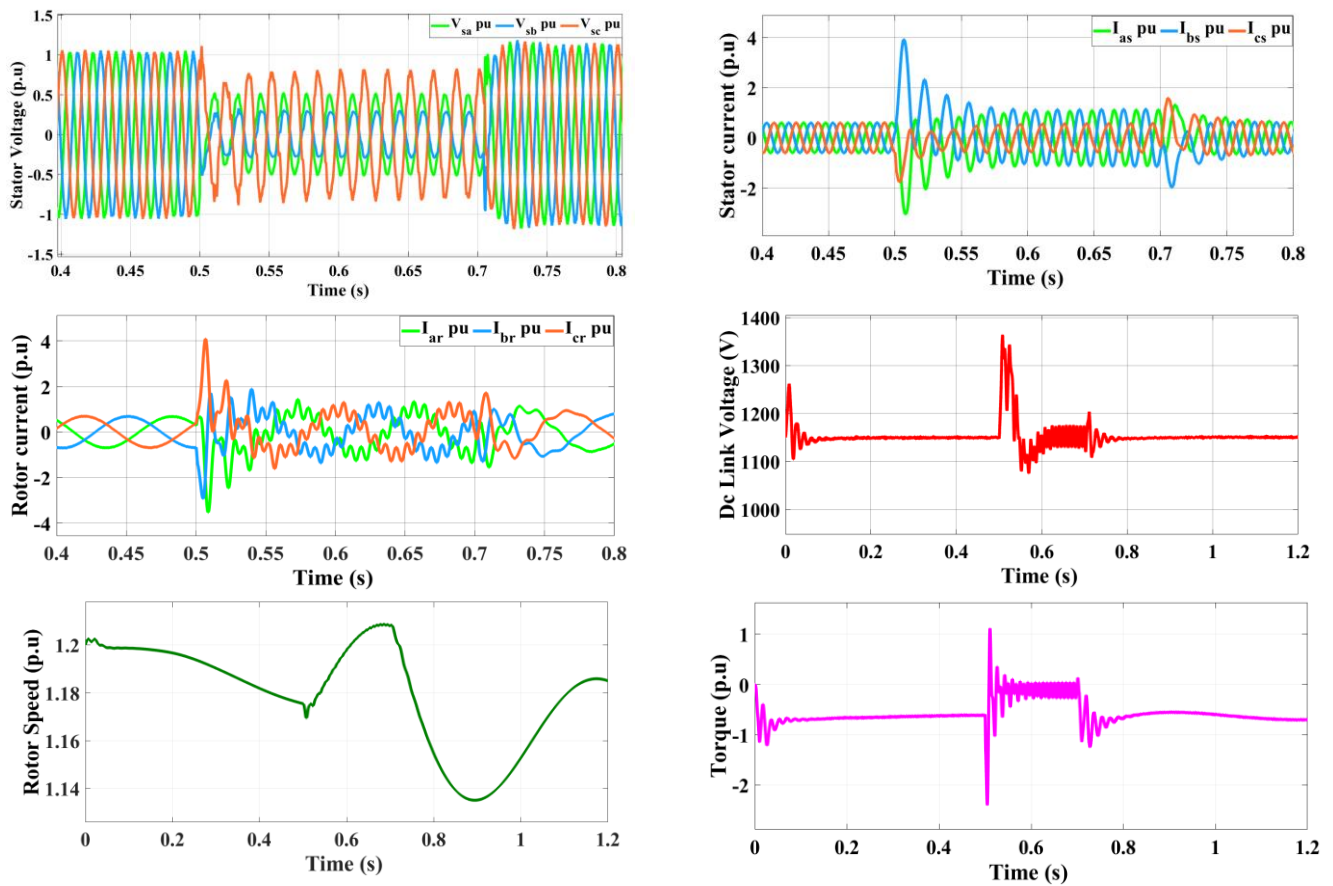**Fig 10** Peak Values of Voltage and Current during Faults
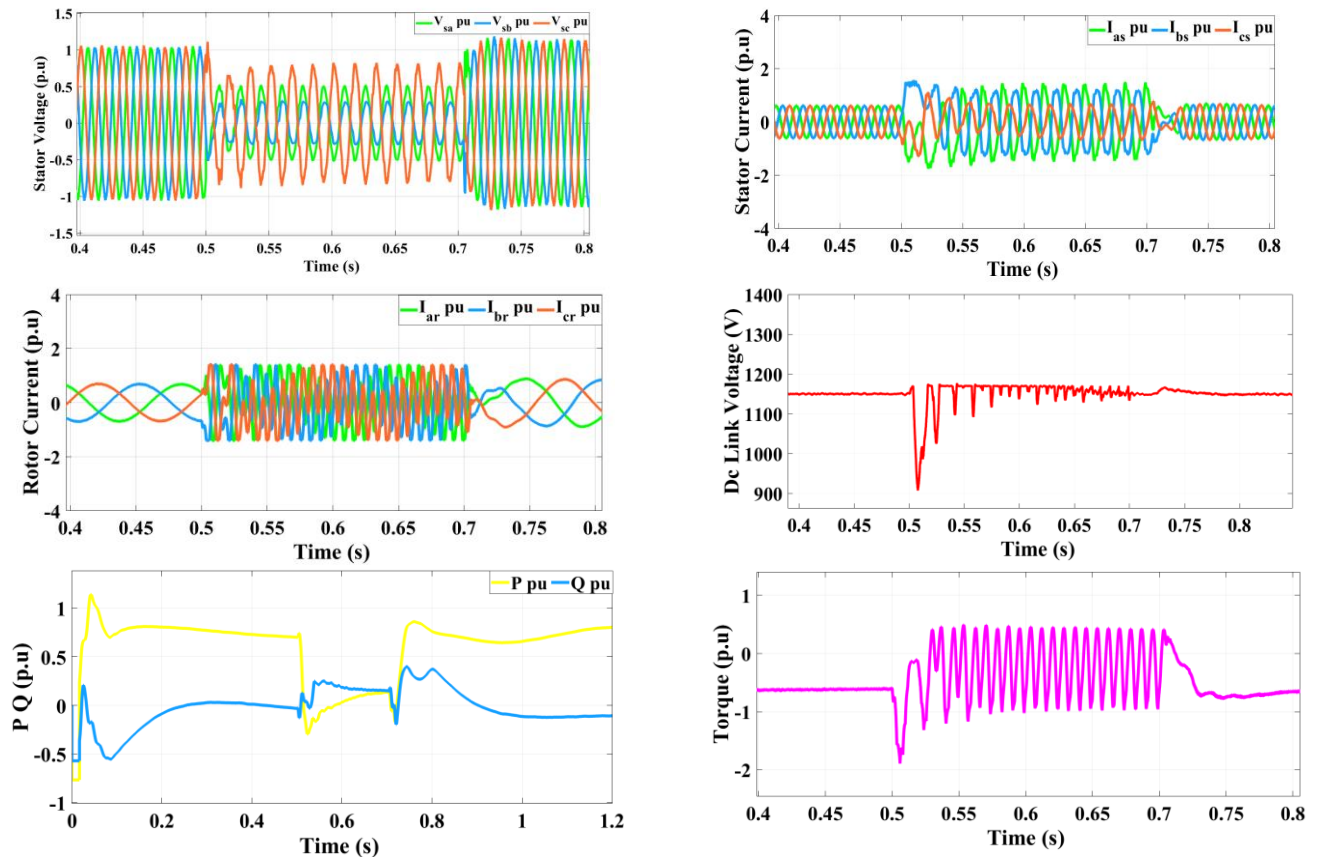**Fig 11** DFIG's dynamic behavior in the absence of a protection system with Asymmetrical Fault (LL)
Fig 12 DFIG's dynamic behavior in the presence of a protection system with Asymmetrical Fault (LL)
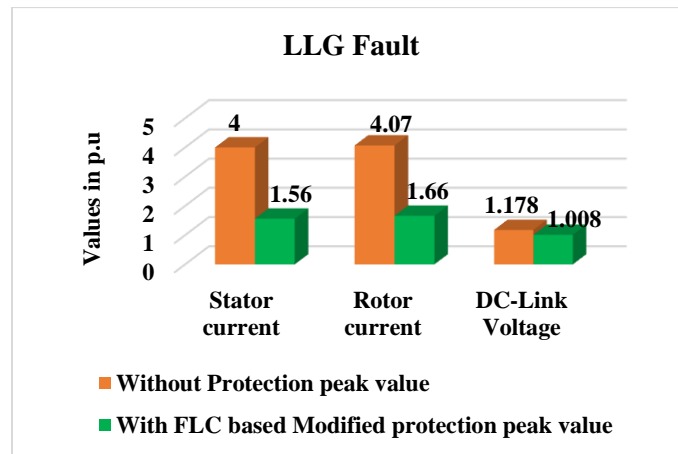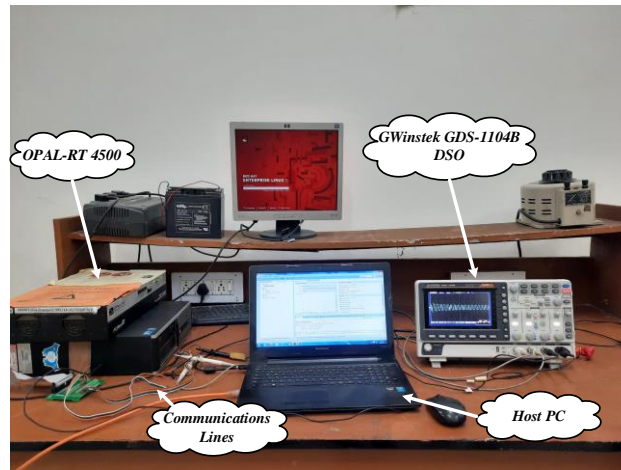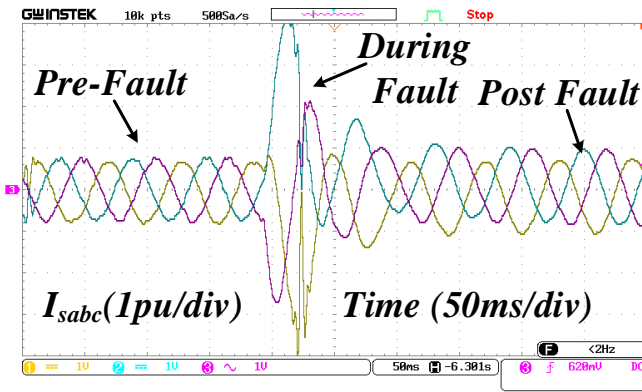**Fig 13** Peak Values of Voltage and Current during Faults
Fig 14 DFIG's dynamic behavior in the absence of a protection system with Asymmetrical Fault (LLG)
Fig 15 DFIG's dynamic behavior in the presence of a protection system with Asymmetrical Fault (LLG)
Fig 16 Peak Values of Voltage and Current during Faults
Fig 17 RTS diagram of FRT of DFIG based WEC system
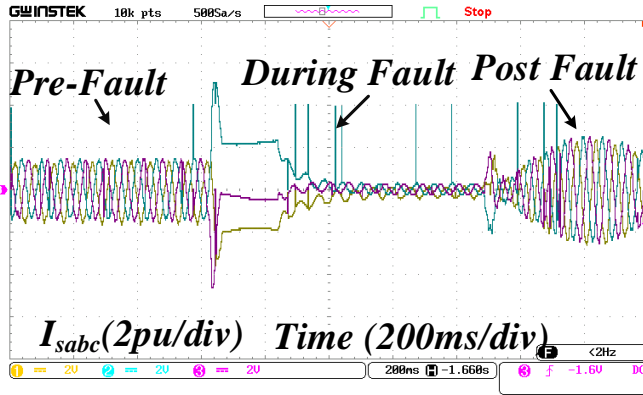**Fig 18** Real-time simulator (RTS) results in the absence of protection system with Symmetrical Fault
Fig 19 Real-time simulator (RTS) results in the Presence of REPRC protection system with Symmetrical Fault
Fig 20 Real-time simulator (RTS) results of an improved FL based protection system with Symmetrical Fault
Fig 21 Real-time simulator (RTS) results of an improved FL based protection system with Asymmetrical Fault (L-L)
Fig 22 Real-time simulator (RTS) results of an improved FL based protection system with Asymmetrical Fault (L-L-G)

Table Content

Table 1 Symmetrical component of the grid voltage under asymmetrical
Table 2 Coordination of Protection Techniques in Various Scenarios

Fig 1 DFIG's stators' flux paths during symmetrical voltage sags (a) prior to sag (b) during sag (c) after sag

(a)

(b)

(c)

Fig 2 DFIG equivalent circuit model exposed to symmetrical voltage sag: (a) natural-machine and (b) forced-machine (c) negative machine.

Fig 3 Flux path of the stator in the event of an asymmetrical grid failure (a) Steady-state after a fault (b) the zero flux state; and (c) the maximum natural flux state.

Fig 4 DFIG with Modified FL-based parallel protection scheme

Fig 5 Model of DFIG rotor equivalent circuit illustrating all protection schemes
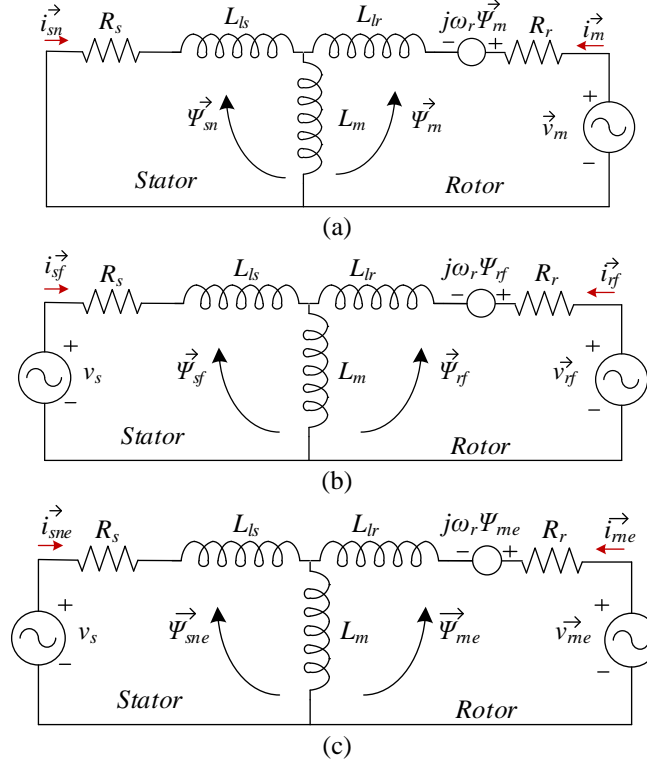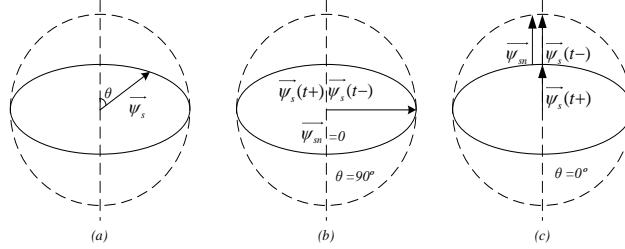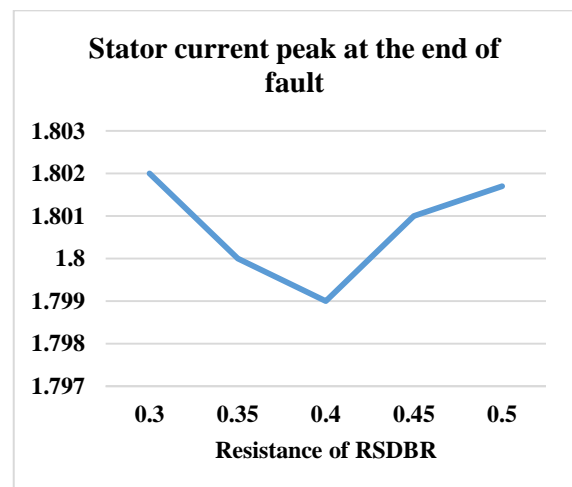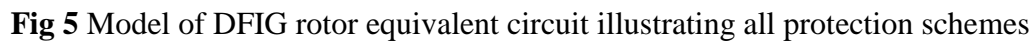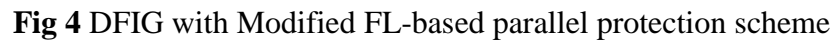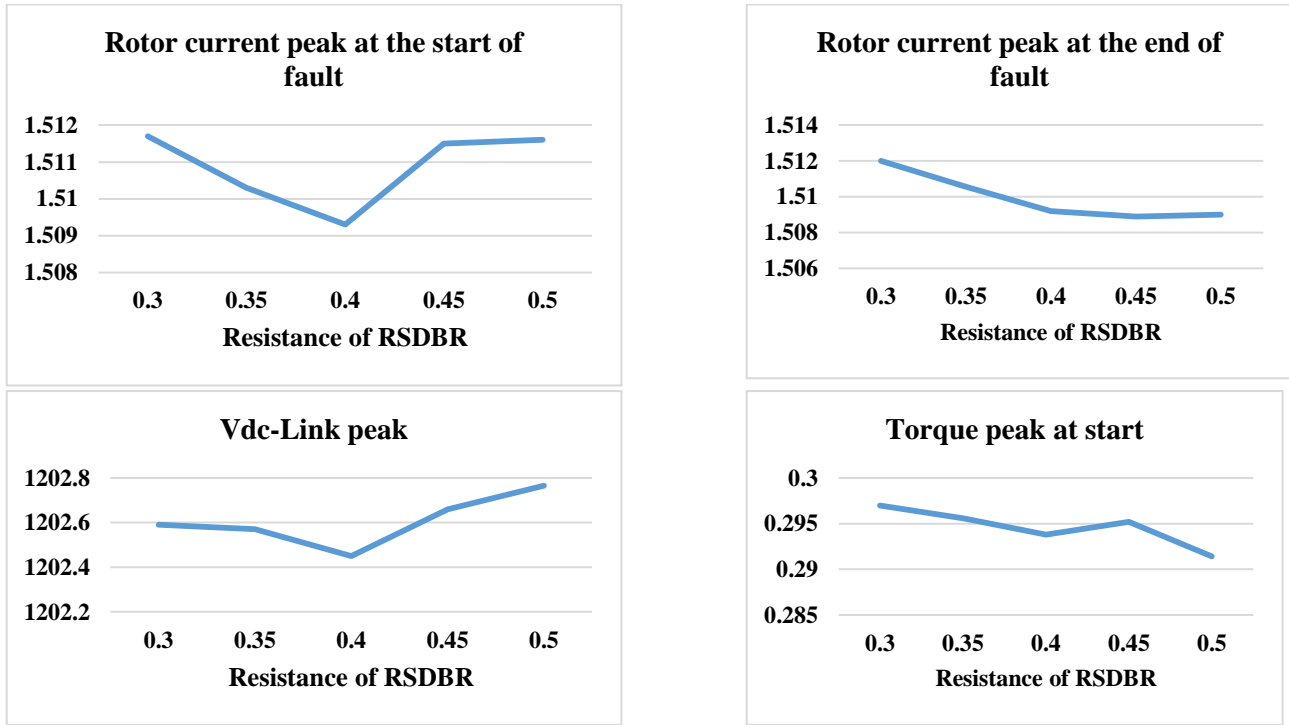
Fig 6 Optmal value of resistance of RSDBR for protection

Fig 7 DFIG's dynamic behavior in the absence of a protection system with Symmetrical Fault

Fig 8 DFIG's dynamic behavior in the presence of Crowbar protection system with Symmetrical Fault

Fig 9 DFIG's dynamic behavior in the presence of Proposed protection system with Symmetrical Fault

Fig 10 Peak Values of Voltage and Current during Faults

Fig 11 DFIG's dynamic behavior in the absence of a protection system with Asymmetrical Fault (LL)

Fig 12 DFIG's dynamic behavior in the presence of a protection system with Asymmetrical Fault (LL)

Fig 13 Peak Values of Voltage and Current during Faults

Fig 14 DFIG's dynamic behavior in the absence of a protection system with Asymmetrical Fault (LLG)

Fig 15 DFIG's dynamic behavior in the presence of a protection system with Asymmetrical Fault (LLG)

Fig 16 Peak Values of Voltage and Current during Faults

Fig 17 RTS diagram of FRT of DFIG based WEC system

(a) Stator Current
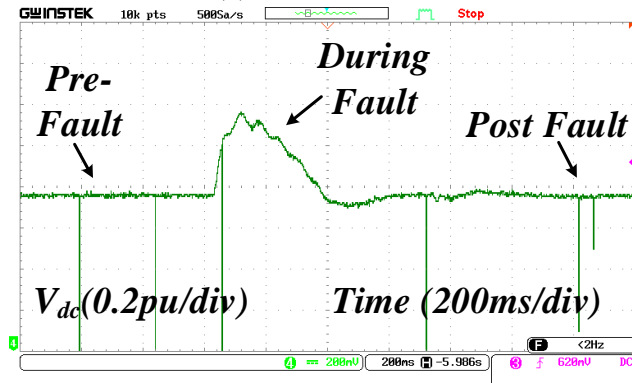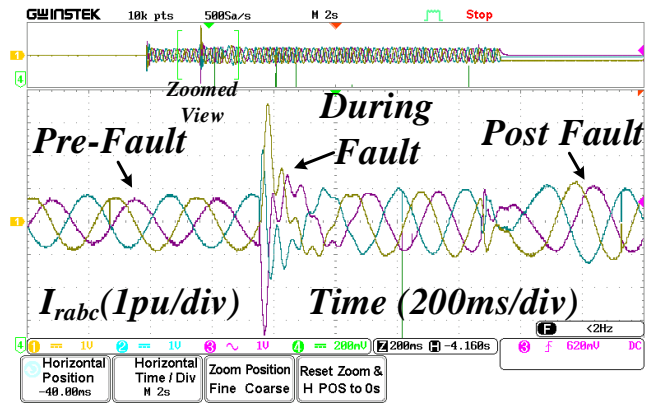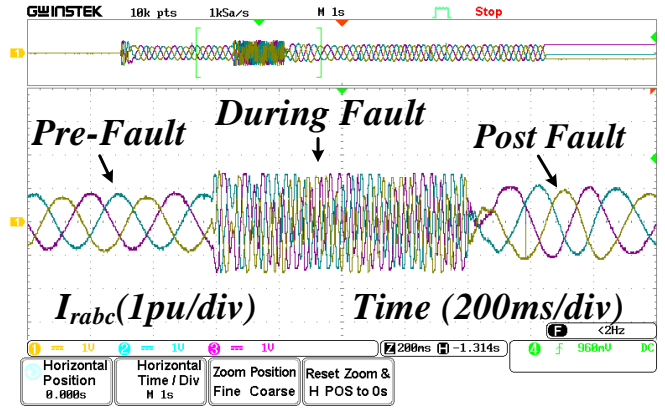

(b) Rotor Current
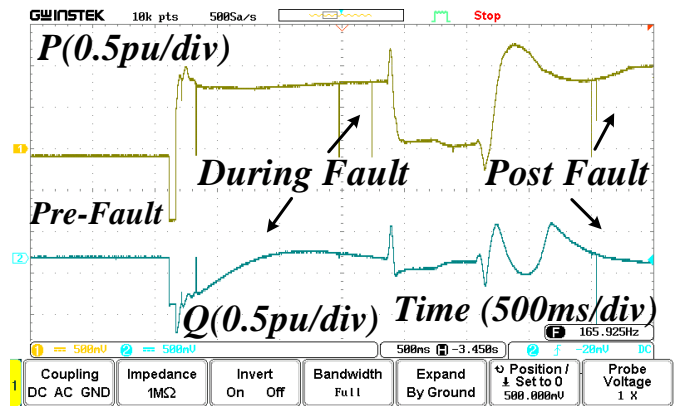
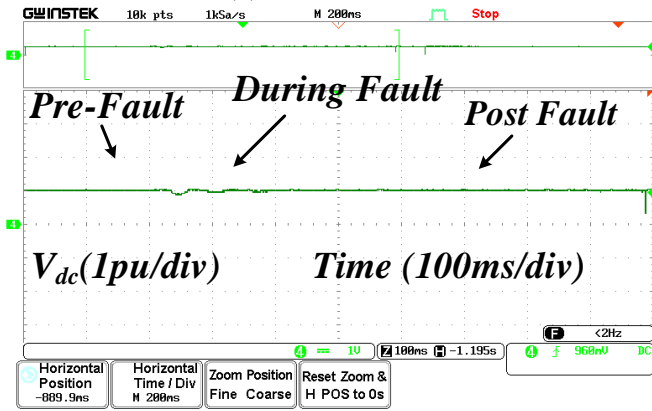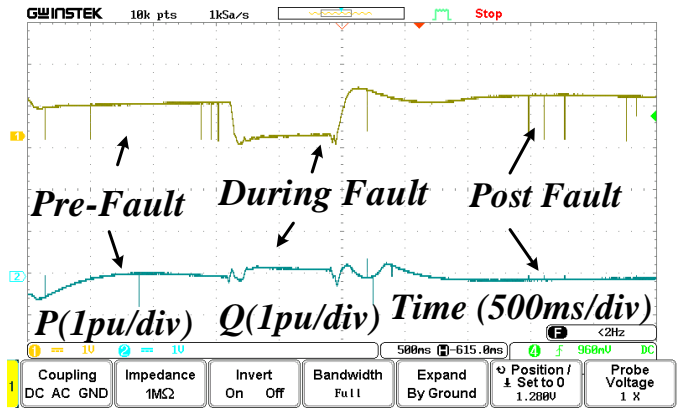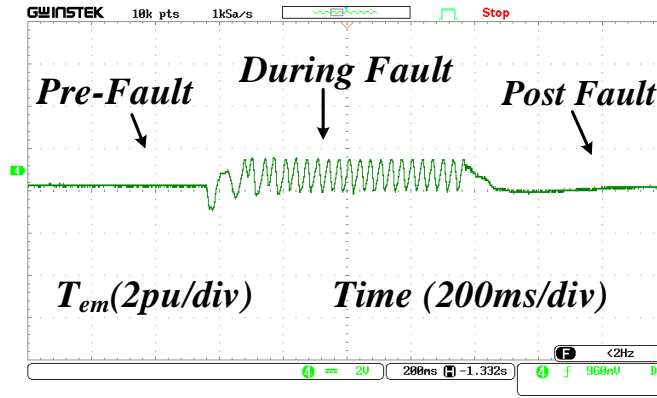(c)Dc Link Voltage

(d) Active and Reactive Power
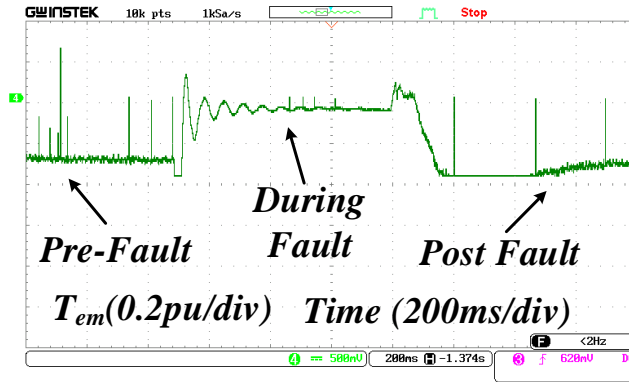
(e) Torque

Fig 18 Real-time simulator (RTS) results in the absence of protection system with Symmetrical Fault
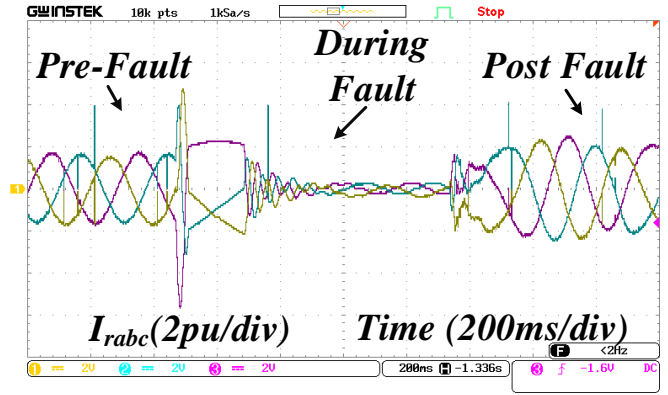
(a) Stator Current
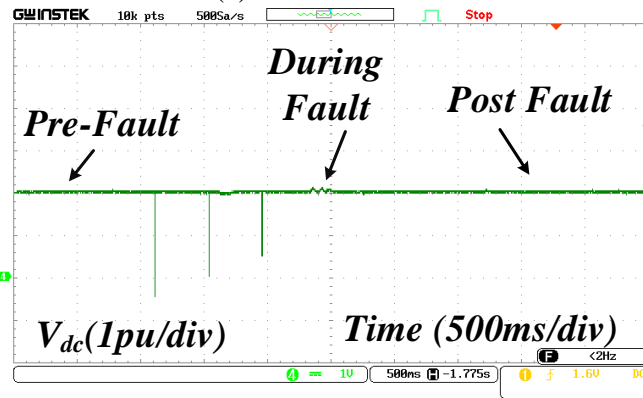
(b) Rotor Current
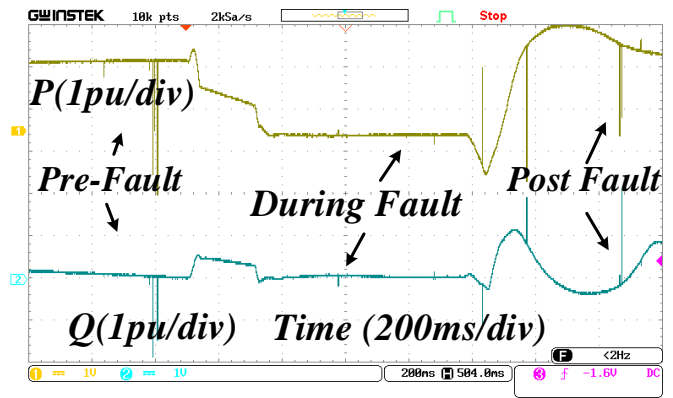
(c)Dc Link Voltage

(d) Active and Reactive Power
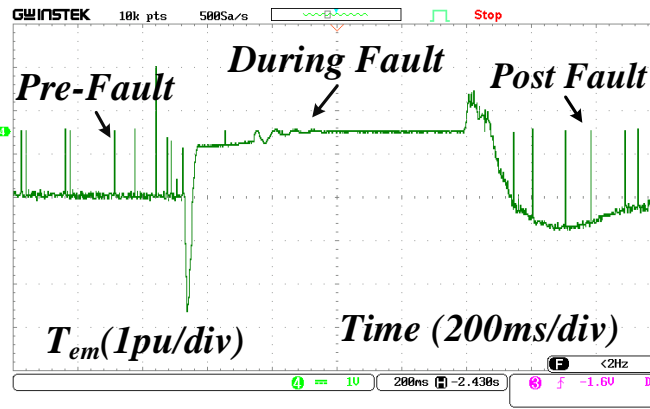
(e) Torque

Fig 19 Real-time simulator (RTS) results in the Presence of REPRC protection system with Symmetrical Fault
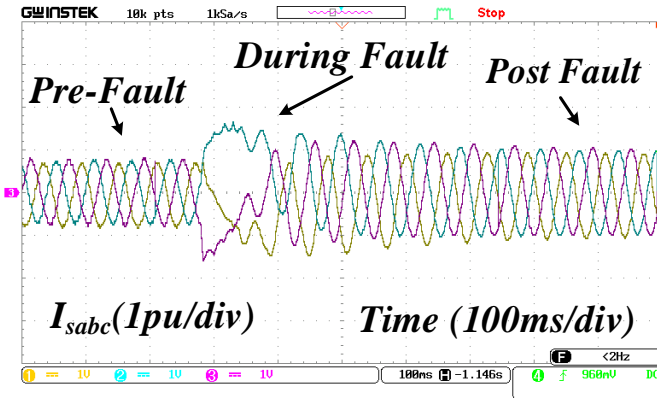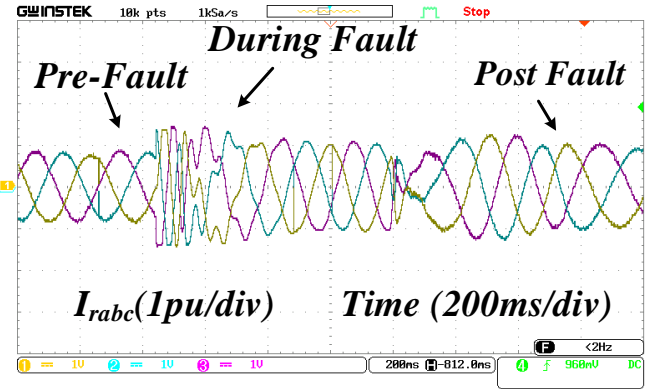
(a) Stator Current
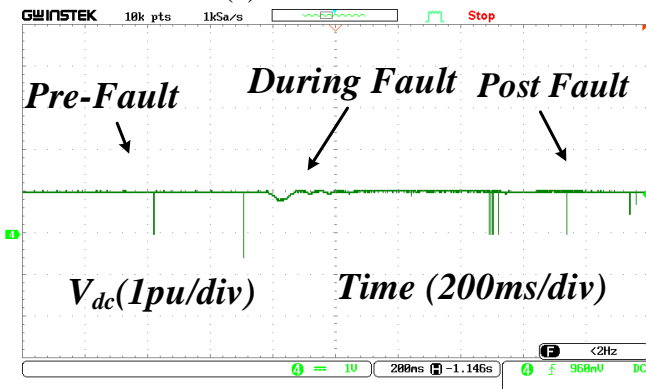
(b) Rotor Current
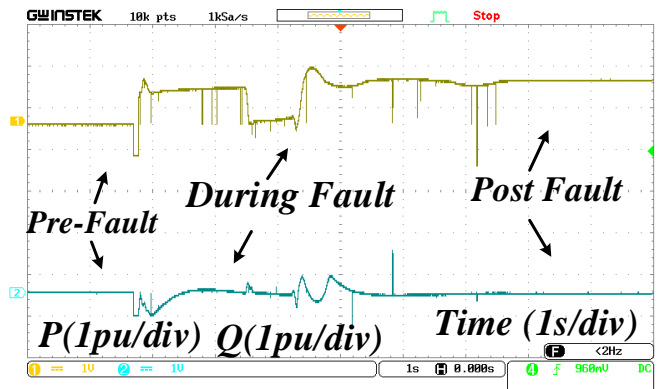
(c)Dc Link Voltage

(d) Active and Reactive Power
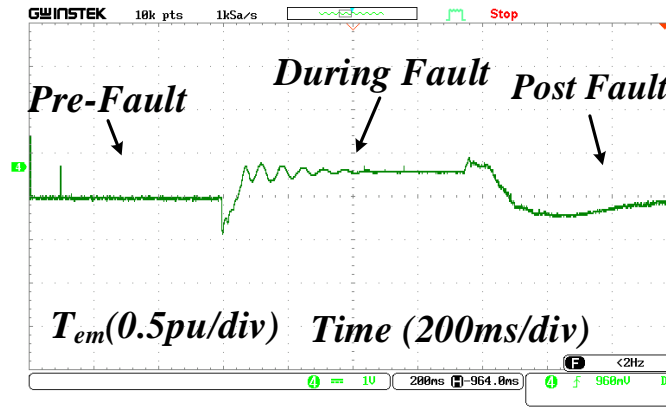
(e) Torque

Fig 20 Real-time simulator (RTS) results of an improved FL based protection system with Symmetrical Fault
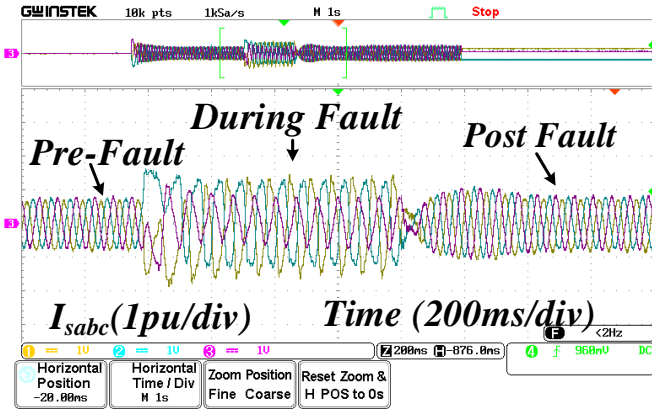
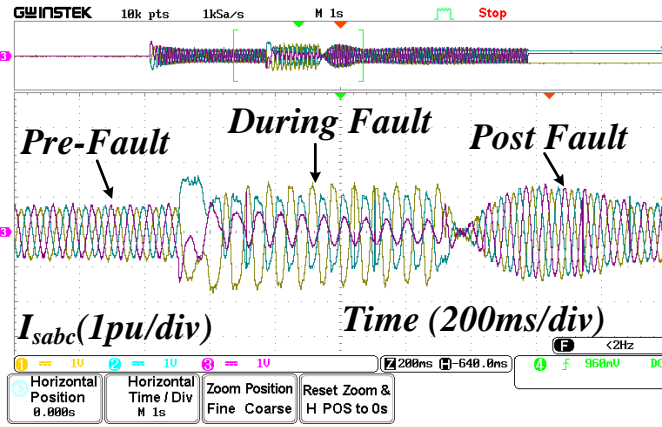(a) Stator Current

(b) Rotor Current

(c)Dc Link Voltage

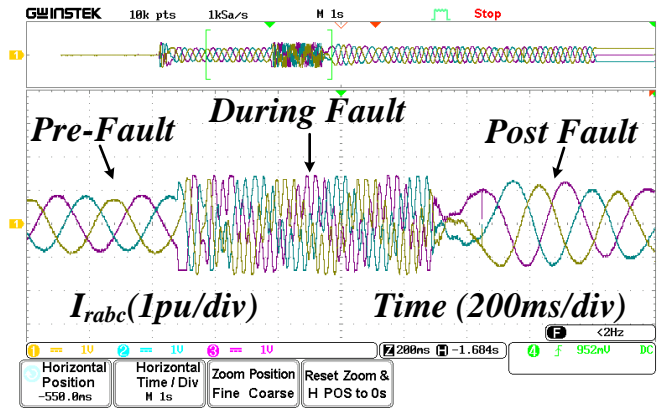
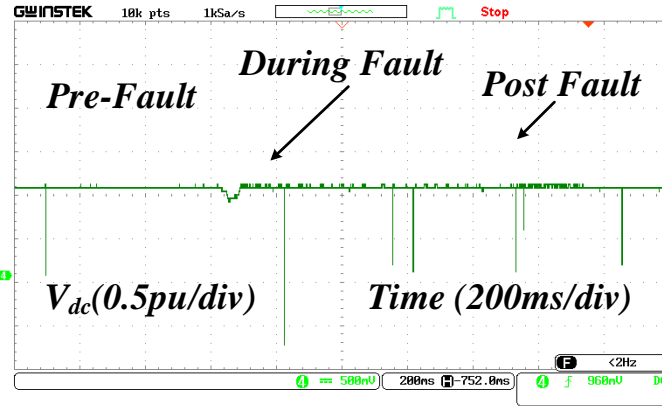(d) Active and Reactive Power

(e) Torque

Fig 21 Real-time simulator (RTS) results of an improved FL based protection system with Asymmetrical Fault (L-L)
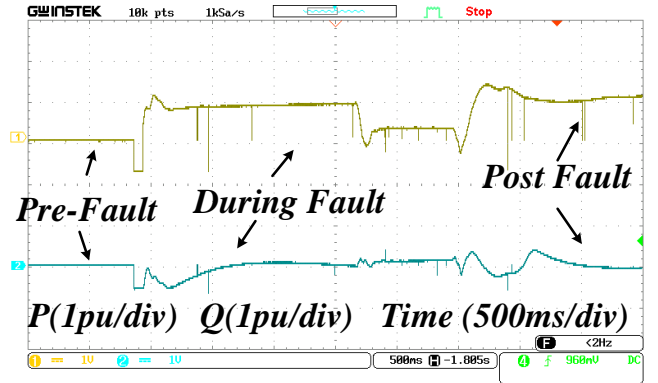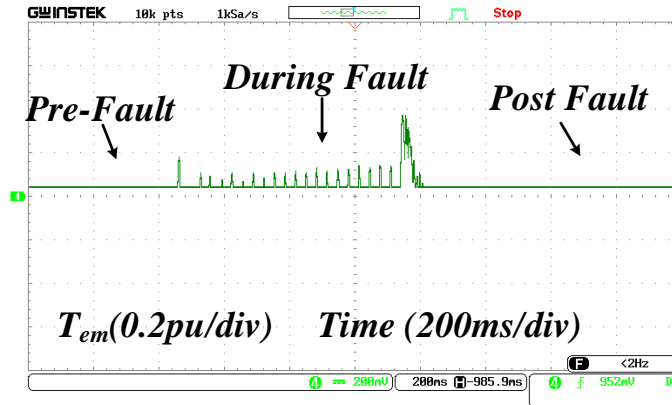

(a) Stator Current

(b) Rotor Current

(c)Dc Link Voltage

(d) Active and Reactive Power

(e) Torque

Fig 22 Real-time simulator (RTS) results of an improved FL based protection system with Asymmetrical Fault (L-L-G)

Fault type	V_s^+	V_s^-	V_s^0
Single-phase to ground	$1 - p/3$	$p/3$	$p/3$
Two-phases	$1 - 2p/3$	$p/3$	0
Two-phase to ground	$1 - p/2$	$p/2$	0

Table 1 Symmetrical component of the grid voltage under asymmetrical [22]

OC[1]	OV[2]	MSP[3]	FPA[4]	SPA[5]	TPA[6]
No	No	-	-	-	-
Yes	No	RSPEC	RSDBR	REPRC	DCBC
No	Yes	DC Link	DCBC	RSDBR	REPRC
Yes	Yes	RSPEC and DC Link	RSDBR	DCBC	REPRC
High OC	No	RSPEC	REPRC	RSDBR	DCBC
	High OV	DC Link	DCBC	REPRC	RSDBR
High OC	High OV	RSPEC and DC Link	REPRC		DCBC

[1] *Overcurrent,* [2] *Overvoltage,* [3] *Most susceptible part,* [4] *First protective action,*
[5] *Second protective action,* [6] *Third protective action*

Table 2 Coordination of Protection Techniques in Various Scenarios